photonics

MDPI

Article

Fundamentals of Determination of the Biological Tissue Refractive Index by Ellipsoidal Reflector Method

Natalia Bezugla [1], Oleksandra Romodan [1], Pawel Komada [2,*], Nataliia Stelmakh [1] and Mykhailo Bezuglyi [1]

[1] Department of Computer-Integrated Technologies of Device Production, Faculty of Instrumentation Engineering, National Technical University of Ukraine "Igor Sikorsky Kyiv Polytechnic Institute", Beresteiskyi Ave., 37, 03056 Kyiv, Ukraine; n.bezugla@kpi.ua (N.B.); oleksandra.romodan@ukr.net (O.R.); n.stelmakh@kpi.ua (N.S.); m.bezuglyi@kpi.ua (M.B.)

[2] Department of Electronics and Information Techniques, Faculty of Electrical Engineering and Computer Science, Lublin University of Technology, 38D Nadbystrzycka Street, 20-618 Lublin, Poland

* Correspondence: p.komada@pollub.pl

Abstract: This paper presents the theoretical fundamentals, prerequisites for creation, and peculiarities of modeling a new method for determining the refractive index of biological tissues. The method uses a mirror ellipsoid of revolution as an optical element to ensure total internal reflection phenomena. This paper thoroughly analyzes the differences in the refractive index of healthy and pathological tissues on a biometric diagnostic basis. The analysis is used to model the measurement setup's parameters. This paper also considers various methods of determining the refractive index of biological tissues based on different principles of physical optics, such as interferometry, refractometry, ellipsometry, and goniophotometry. It systematizes typical optical elements of total internal reflection that can be used in goniophotometry. It justifies the selection of the element base for the goniometric installation based on the ellipsoidal reflector method. A simulation of the installation operation was carried out for various parameters of the ellipsoidal reflector, ensuring the measurement of the biological tissue refractive index from 1.33 to 1.7. This paper also proposes a constructive solution for manufacturing an ellipsoidal reflector of the required configuration.

Keywords: refractive index; total internal reflection; ellipsoidal reflector; biological tissue; image processing; CCD camera; optimization

check for updates

Citation: Bezugla, N.; Romodan, O.; Komada, P.; Stelmakh, N.; Bezuglyi, M. Fundamentals of Determination of the Biological Tissue Refractive Index by Ellipsoidal Reflector Method. *Photonics* **2024**, *11*, 828. https://doi.org/10.3390/photonics11090828

Received: 19 July 2024
Revised: 26 August 2024
Accepted: 28 August 2024
Published: 2 September 2024

Copyright: © 2024 by the authors. Licensee MDPI, Basel, Switzerland. This article is an open access article distributed under the terms and conditions of the Creative Commons Attribution (CC BY) license (https://creativecommons.org/licenses/by/4.0/).

1. Introduction

Absorption, scattering, refraction, and reflection processes characterize light's interaction with biological media. Both for the classical wave theory and its development [1,2], when dielectric and magnetic permeability are fundamental, and for the theory of radiation transfer [3–5], when the absorption coefficient, the scattering coefficient, and the scattering anisotropy factor are fundamental, the refractive index n(λ) values are the most significant and are crucial values characterizing the spectral optical properties of the media. For homogeneous transparent media, the refractive index (RI) value is considered the number that quantitatively establishes the reduction index, the speed of light inside the media relative to the speed of light in a vacuum [6]. However, biological tissues (BTs) are significantly heterogeneous and significantly absorb light [6]; therefore, the RI is interpreted as a complex number, with the real part having the most significant influence on refraction and the speed of light and the imaginary part characterizing absorption and scattering [7,8]. At the same time, both components have approximately the same effect on light reflection [8]. When studying the optical properties of BTs, attention is usually paid to the real part of the complex RI since, in most cases, the imaginary part is a small value [8]. The following literature review mainly focuses on recent studies determining the RI's real part. It considers the features of light refraction by biological tissues rather than its attenuation. Snell's law is the geometric basis for setting and determining the angles of incidence and

refracted beams; it practically does not allow measuring the parameters that would allow determining the imaginary part of the RI. In general, the calculation of the imaginary part is quite complicated since the attenuation coefficient of the media, which is a characteristic of the decrease in the power of the incident light, is determined by the sum of the scattering and absorption coefficients of BT [9]. These coefficients cannot be measured; the process of their determination is reduced to solving the inverse problem of light scattering optics by optimization methods for one of the methods of biophotonics (adding-doubling [10], Monte Carlo [5], and others).

In biological tissues, the value of the RI varies significantly. So, for example, the RI values for the whole cell vary from 1.346 to 1.478, and for subcellular structures, 1.343–1.70 [11]. In general, the RI value for biological tissues, as a rule, is 1.33–1.55 [12–14]. Variations in RI can potentially be indicators of health status, as morphological changes occur in these structures during the progression of many diseases [15]. That is why this constant is especially important for medical diagnosis and therapy and can be used, for example, as a marker of cancer [6,7,15–17], because cancer makes the tissue more heterogeneous, due to which the light scattering by the tissue increases [17]. At three wavelengths of the visible spectrum (450 nm, 532 nm, and 632.8 nm) and two near-infrared wavelengths (963 nm and 1551 nm), changes in refractive properties between normal and malignant tissues of the colon and rectum were observed [16]. The values of refractive indices were (964 nm): normal mucosa (caecum) $n = 1.329$; benign tumor (adenoma) $n = 1.347$; normal mucosa (rectum) $n = 1.337$; and malignant tumor (adenocarcinoma) $n = 1.315$. In [17], the RI (530 nm) was used to detect prostate and breast tumors. It was found that the progression of cancer significantly changes the organization of tissue cells, evidenced by the consistently more excellent dispersion of the RI in tumors than in healthy tissues. With the help of phase imaging [16], the dispersion of the RI for healthy liver tissue was determined, which is 0.0190, while for the tumor, it is 0.0205. For the kidney, the value for the healthy tissue is 0.0156 for the tumor it is 0.0174). Malignant areas also show consistently higher values of the anisotropy coefficient [16].

The methods of determining the RI can be classified according to the physical phenomenon (interference, total internal reflection (TIR), refraction, transmission, reflection) and visualization of the obtained data (1D, 2D, 3D)—the measurement technique basis or the optical devices used [18]. Michelson interferometry [18] and its applied development in the methods of low coherence interferometry and optical coherence tomography (OCT) [19–21] make it possible to determine the changes in the RI in three dimensions (3D), which allows for studying heterogeneous biological media (for example, skin [19], cornea [20], enamel, and dentin [21]). However, these methods may have some limitations. A fixed wavelength of the light source [22–24], complex 3D reconstruction algorithms, and mechanisms for focusing the laser beam on the front and back surfaces of the sample can be challenging to implement in biological tissues [20]. The study of transmission, refraction, and reflection phenomena is used in refractometry and ellipsometry. Refractometry mainly obtains the deflection angle value on the media's surface [18]. When using ellipsometry, RI is measured based on the change in polarization of light during transmission/reflection [18,25]. The main disadvantages are the functional limitations that allow these methods to determine the RI of only the surface layer or fragile BT samples. Various variations in microscopy and spectroscopic methods, polarimetric measurements, the method of minimum deviation, combinations of several methods, etc., are based on these physical phenomena. With the microscopy methods, 2D visualization of the RI of biological organelles and tissues can be obtained [6]. The simplest and, simultaneously, the most accurate methods are based on the phenomenon of total internal reflection of TIR [22]. The TIR method is the basis of the traditional Abbe refractometer, which operates within a relatively wide scale of refractive indices and usually uses a light source emitting a clear spectral line in the visible range [24]. Although this method is considered the most accurate, it is only suitable for in vitro studies of the RI.

Measuring the RI of biological tissues based on the TIR phenomenon is also the basis of goniometric (goniophotometric) methods [18]. The measurement base of these methods contains a rotary system and an optical element with an RI that is more significant than the predicted BT RI. The TIR optical element can consist of two right-angled prisms (according to the Abbe refractometer principle, Figure 1a) [26] or have the interface between the lens and tissue sample changed from a parallel plane model to a specific cylinder model (Figure 1b) [12]. Other options use mono-elements in the form of an equilateral triangular prism (Figure 1c) [7,9,16,22,25,27–29], a cylindrical prism (Figure 1d) [30–32], or a mirror ellipsoid of revolution (Figure 1e) [32,33]. Regardless of the optical element used, the essence of the goniometric method boils down to moving one or more circuit elements (light source, optical element, and photodetector) to register the critical angle at which the TIR phenomenon is observed. A biological tissue sample can be located between two prisms (Figure 1a,b) when measurements are permissible in vitro or under an optical element when the research conditions allow an in vivo experiment (Figure 1c–e).

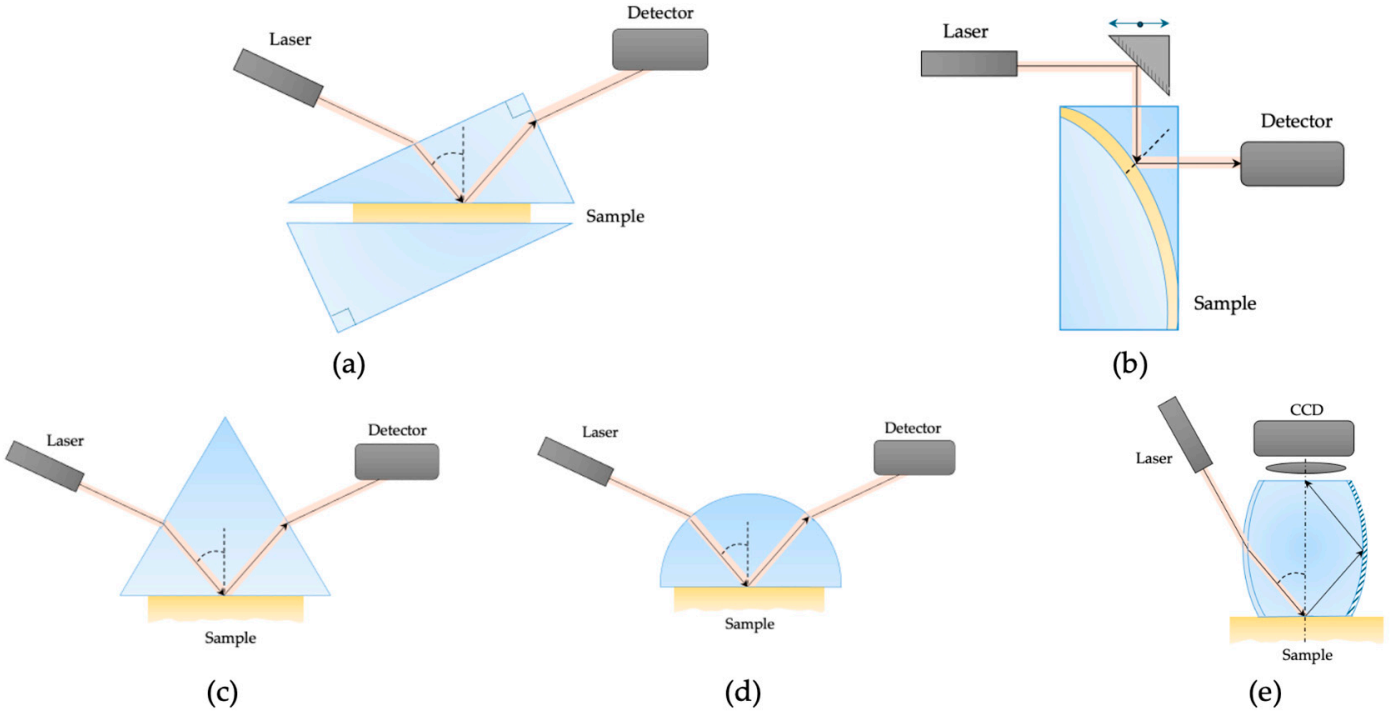


Figure 1. Optical systems for goniometric methods of measuring the BT RI: right-angled (**a**) and cylinder (**b**) prism systems, equilateral triangular prism (**c**), semi-cylindrical prism (**d**), ellipsoidal reflector (**e**).

In most cases, the prism (or prisms) and the sample (Figure 1a,c) are rotated using a goniometric adjustment relative to the incident beam until the moment when the beam hits the opposite surface of the prism reaches a critical angle [26,28]. In some cases (Figure 1a,c,d), the critical angle is achieved by rotating only the light source [30] or longitudinally moving additional optical elements (prism in Figure 1b) [12]. In paper [9], a right-angled prism was placed on a goniometer that rotated with a stepper motor, and the laser beam fell on the side of the prism. Similarly, in the paper [26], two identical right-angled prisms were placed in the center of the rotating goniometer platform. In the experiment in [29], the laser and the detector rotated synchronously. In [30], two goniometers were used: the first goniometer to control the rotation of the "prism–sample" complex and the second to control the rotation of the measuring device.

In the goniometric method, a key component is an ellipsoidal reflector cut along the focal planes orthogonally to the semi-major axis (Figure 1e) [33,34]. When used with the TIR optical element, this reflector allows only the light source to move while the sample

and photodetector remain stationary. This unique setup enables in vivo research and facilitates the registration of the scattered component in back-reflected light, a crucial step in determining the imaginary part of the complex number of the biological tissue RI.

The main goal of this work is to develop the structural and functional principles of the goniometric method for modeling the determination of the RI of biological tissues using an ellipsoidal reflector.

2. Materials and Methods

The main elements of goniometers are a light source, an optical system, and a detector. The mutual placement of these elements using a rotary system allows for fixing and measuring the angles of light refraction that pass through the BT sample under investigation. We characterize the features of these components in biological tissue RI determination by the ellipsoidal reflector method.

Light source. Without excluding the possibility of using radiative sources typical for goniometric systems (lamps, halogen light sources, LEDs, and others), for the implementation of the proposed idea, it is proposed to use a highly stable and affordable He-Ne laser of continuous action (LGN-208 or analogs) with a wavelength of unpolarized radiation of 632.8 nm. It is caused by the properties of the optical radiative source itself and by the amount of literature data on measuring the BT RI in the visible range [7,12,16,18,25,26,29–34]. Various approximation models were obtained to compare and evaluate the RI values at different wavelengths [18]. Among these models, the Cauchy relation is an empirical model often used to describe the wavelength dependence of the RI for various substances, including biological tissues [26]. Generally, the RI values of biological tissues (e.g., fat, muscle, liver, body fluid) continuously decrease with increasing wavelength [32]. The light source is moved in the measurement scheme, and the photodetector remains stationary, facilitating noninvasive measurement of the human skin RI, for example.

Photodetector. As a rule, goniometric-type systems use a wide range of optical radiation receivers, including photodiodes [7,9,25,30], fiber-optic detectors, UV/IR converters, high-speed cameras [22], photon detectors [25], and CCD cameras [33,34]. Considering the peculiarities of the optical biometry of media by the ellipsoidal reflectors method [34–36], the most appropriate choice would be a monochrome CCD camera DMK 21AF04.AS model (The Imaging Source, LLC, Charlotte, NC, USA) with an adjustable gain level with a Sony ICX098BL sensor (Sony Corporation, Tokyo, Japan) to allow it to receive a video stream of photometric images at a speed of up to 60 images per second and with a resolution of 640 × 480 (0.3 MP).

Optical element. An ellipsoidal reflector (ER) is an ellipsoid of revolution, with the transparent material's RI greater than 1.7. The ER is truncated orthogonally concerning the major semi-axis along the planes containing the focal points F1 and F2, and the side surface contains a coating that provides acts of mirror reflection inside the reflector (Figure 2a). The ER in Figure 2b was made of clear glass to measure the RI of biological tissue in the visible (380–750 nm) and near-infrared (750–2500 nm) spectra. Since the RI of biological tissues can be as high as 1.7, the RI of glass must be greater than this value to ensure that the conditions of Snell's law are met. Flint glass is a material that meets these conditions, as its RI varies from 1.45 to 2.00 [35]. Traditionally, flint glass contains lead oxide (up to 60%). However, in modern chemical compositions, lead oxides are often replaced by other metal oxides, such as titanium dioxide or zirconium dioxide, without significantly affecting the optical properties of the glass. Crown glass also meets the conditions, particularly BAK-4 (barium-coated glass, code 569560) [36].

For a mirror coating of about 100 nm, we recommend using silver, gold, or copper, which provide high reflectivity in the visible and near-infrared ranges [37]. The azimuthal angle value $\Delta\varphi$ is chosen to ensure the width of the tape d, necessary for the desired introduction of a corresponding radius laser beam. For the introduction of optical radiation into the ER body, on its side there is a ribbon-like element free of coating, formed by

sectors of an ellipsoid, which are symmetrical to its major semi-axis and lag each other by a slight azimuthal angle Δφ (Figure 2b). The azimuthal angle value Δφ is chosen to ensure the width of the tape d, necessary for the desired introduction of a corresponding radius laser beam.

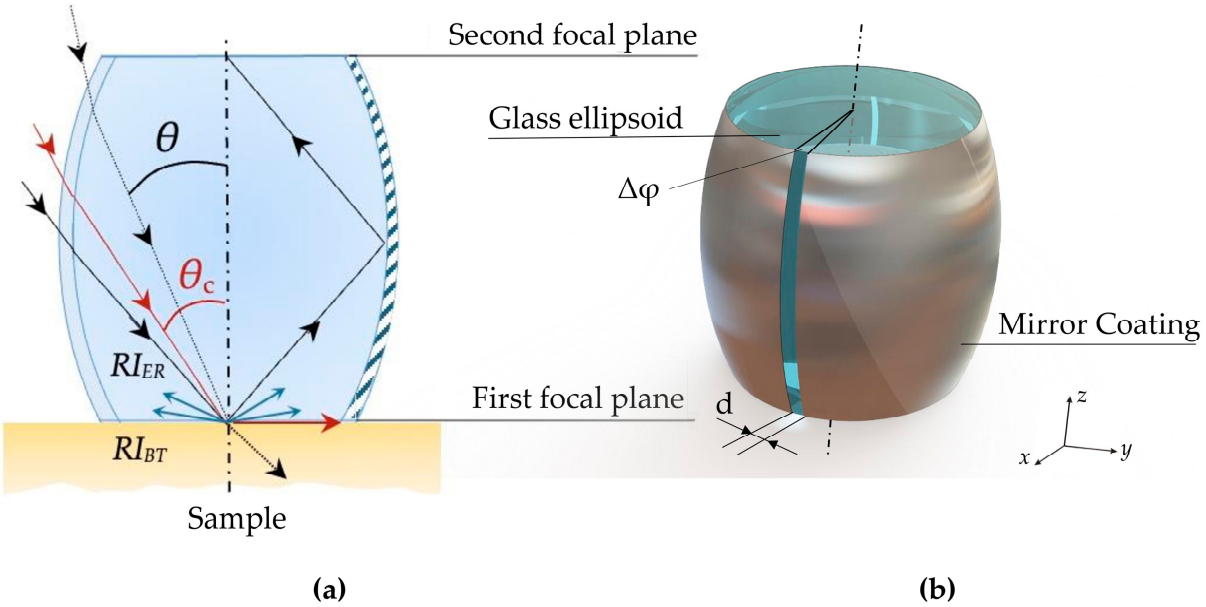


Figure 2. Postulates of biological tissue RI determination with ER method: (**a**) total internal reflection and (**b**) ellipsoidal reflector 3D design: θ is the angle of incidence on the surface of the BT sample, θ_c is the critical angle (angle of total internal reflection of the BT sample), RI_{ER} is the RI of ER material, RI_{BT} is the RI of biological tissue, Δφ is the azimuthal angle, d is the width of the ribbon-like element.

The RI determination. As in the case of goniometric systems with optical elements in the form of prisms, the study of the phenomenon of total internal reflection using a mirror ellipsoid of revolution (Figure 2b) is designed to record the critical angle θ_c of light falling on a biological tissue sample (red ray in Figure 2a). At the same time, diffuse scattered light in the reverse direction (blue color in Figure 2a) will be recorded by the CCD camera with varying degrees of intensity depending on the angle of incidence ε on the ER side surface. The diffuse component, which will enter the camera aperture after reaching the critical angle of incidence, will form the imaginary part of the complex number of the BT RI. The relation between the angles ε_1, θ, θ_c, and the refractive indices of the glass ellipsoid material RI_{ER} and the biological tissue RI_{BT} is determined by Snell's law for the corresponding optical media boundary. In Figure 2a, the black color shows the beam whose incidence angle exceeds the critical angle θ_c, as in the case of biological tissue. In this case, the reflected beam stops "sliding" along the "glass ER—BT" boundary, which coincides with the RE first focal plane, and falls on its side, opposite to the localization of the ribbon-like element. Next, the black beam is reflected from the side of the ER and is directed to the second focal plane, which is projected onto the CCD camera photo-sensitive plane. At the same time, it is assumed that the measuring system is in the air with RI = 1.

To continue explaining the idea of implementing the method, we will consider the operation of the functional scheme of the goniometric system with an ellipsoidal reflector for measuring the BT RI (Figure 3).

The fall of the laser beam on the side surface of the ER occurs based on the central premise of the method implementation—the refracted beam enters the first focus of the F1 reflector. For this, the laser must have degrees of freedom that provide two specific movements. The first is the movement in the yz plane along the generating ellipsoid, which is determined by the eccentricity e value, the focal parameter p [34,38,39], and the geometric distance L of the movement mechanisms from the edges of the reflector. The

second is rotation around the x-axis to ensure the necessary coordinates of the laser beam entry point into the reflector at height h. These specific movements are provided by the electromechanical unit EMU connected to the control system and designed for stable feedback to the processing unit. The optical-mechanical system of this measuring device is adjusted so that the laser beam moves parallel to the z-axis along the center of the ER ribbon-like section with a width of *d*.

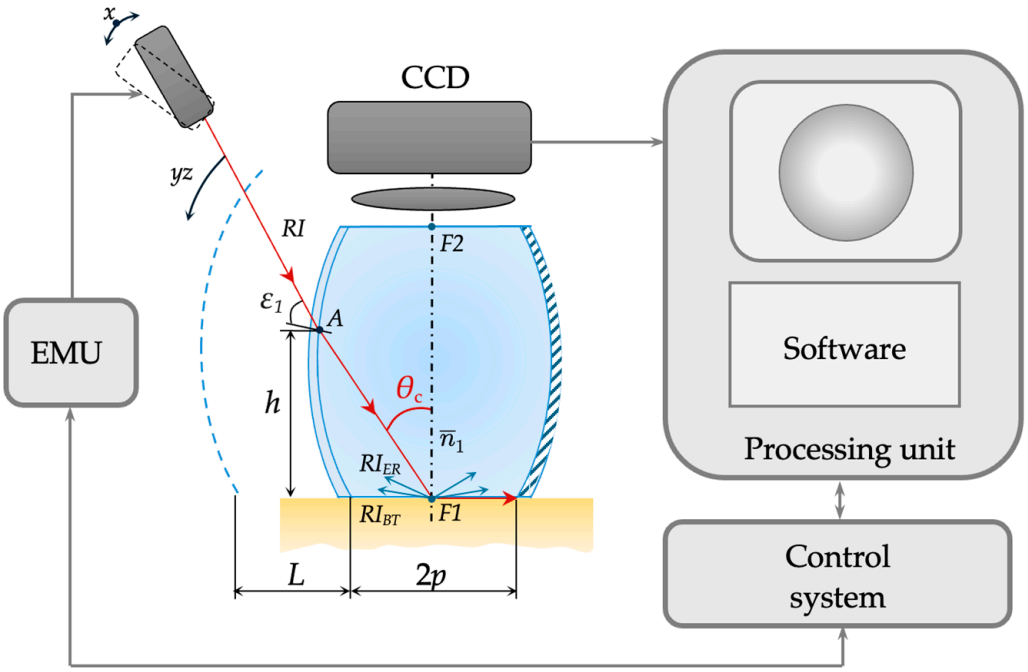


Figure 3. Functional scheme of a goniometric system with an ellipsoidal reflector for measuring the RI of biological tissues: EMU—electromechanical unit, ε_1—incidence angle on the ER side surface, *h*—the beam entrance height into the ER, *L*—distance from the movement mechanisms to the edges of the reflector, *RI*—RI of environment, *F*1 and *F*2—first and second focus of ER, *p*—focal parameter.

The mathematical basis of the proposed method using an optically transparent ER with mirror coating as a TIR element is the direct problem of modeling the light propagation in the laser direction. In this case, it is advisable to start the calculation not from the value of the critical angle (as provided by the instrumental implementation) but from the beam impact point along the ribbon-like section of the reflector. The values determining the beam incidence point on the ER lateral surface are the incidence angle ε and the height *h* (Figure 3). The ER design parameters, which determine the technological principles of its manufacture [34], include the focal parameter *p* and eccentricity *e*, which are used to calculate the minor *a* and the major *b* semi-axis, as well as the focal distance *f*, which define the ellipsoid of revolution mathematically [36]:

$$a = \frac{p}{\sqrt{1-e^2}}, \quad b = \frac{p}{1-e^2}, \quad f = b \cdot e \tag{1}$$

The position of point *A* of the beam falling on the ER side surface, provided that the center of the Cartesian coordinate system is placed in the center of the ellipsoid of revolution (Figure 3), is determined based on the following formulas:

$$y_A = a \cdot \sqrt{1 - \frac{{z_A}^2}{b^2}}, \quad z_A = h - f \tag{2}$$

where *a*, *b*, and *f* are the ellipsoid parameters calculated by Formula (1).

The direction of propagation of the refracted beam at point *A* determines the position of the point of its intersection with the ER first focal plane (at the same time, the mathematical

calculation is justified only for the case when the vector of the refracted beam will cross the first focal plane, and not be directed to the opposite side surface of the reflector). To find this point, it is necessary to determine the position and length of the normal vector $\overline{n}$ at point A:

$$y_n = \frac{2 \cdot y_A}{a^2}, \quad z_n = \frac{2 \cdot z_A}{b^2}, \quad \|\overline{n}\| = \sqrt{{y_n}^2 + {z_n}^2} \tag{3}$$

The vector of the beam refracted at point A will be determined based on the coordinates of this point (2) and the direction cosines of the vector $\overline{R}(\cos\alpha_R, \cos\beta_R, \cos\gamma_R)$ and the normal vector $\overline{n}$ (Figure 4).

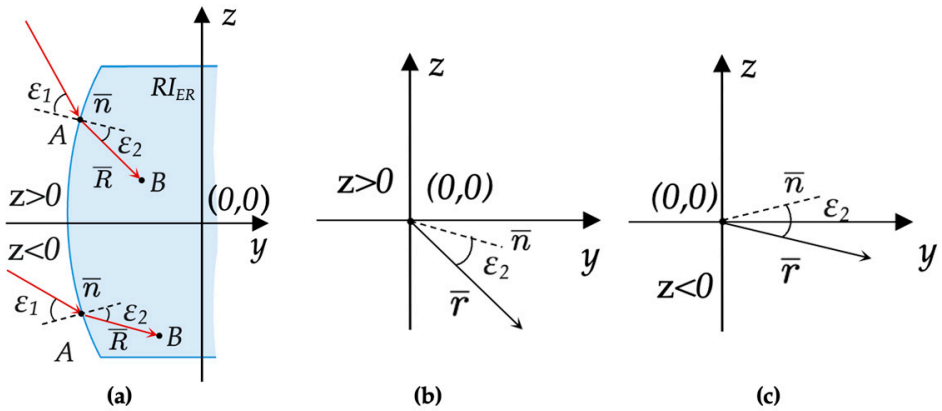


Figure 4. The position of the refracted beam vector $\overline{R}$ relative to the Cartesian coordinate system: (**a**) on the ER lateral surface depending on the position along the oz axis and the position of the unit direction of the refracted beam vector at z > 0 (**b**) and z < 0 (**c**).

At the same time, considering the postulates of the law of refraction of light, the direction cosines of the two-dimensional space will be significant at $\cos\alpha_R = 0$, and the angle between the oy axis and the refracted vector to the normal will be determined as:

$$\cos\beta_R = \frac{y_n}{\|\overline{n}\|} \quad \cos\gamma_R = 1 - \cos\beta_R \tag{4}$$

It is necessary to consider the conditions that depend on the position of the incidence point of radiation, mainly whether it is in the positive (Figure 4b) or negative (Figure 4c) range to the oz axis to obtain the formula for any point belonging to the vector. Then, the position of the unit refracted vector inside the ellipsoid, depending on the conditions, will be determined from the following expressions:

$$\begin{array}{l} z_A < 0, \;\; y_r = \cos(\varepsilon_2 - a\cos(\cos\beta_R)); \;\; z_r = \cos(90 - \varepsilon_2 + a\cos(\cos\beta_R)); \\ z_A > 0, \;\; y_r = \cos(\varepsilon_2); \;\; z_r = \cos(90 - \varepsilon_2 - a\cos(\cos\beta_R)); \\ z_A = 0, \;\; y_r = \cos(\varepsilon_2); \;\; z_r = \cos(90 - \varepsilon_2); \end{array} \tag{5}$$

Hence, through the found values of the unit direction vector $\overline{r}(y_r, z_r)$ and the point $A(y_A, z_A)$ coordinates, we find the point B (Figure 4a), which belongs to the refracted vector $\overline{R}$:

$$y_B = y_r - y_A, \quad z_B = z_r - z_A \tag{6}$$

Now, it is possible to calculate the point C position of the intersection of the refracted beam with the ER first (lower) focal plane, which is in contact with the biological tissue sample under study. To do this, we equate the equation of the line passing through two points, A and B, and the equation of the lower focal plane of the reflector and find the necessary point C coordinates:

$$\begin{cases} z_C = -f \\ y_C = \frac{(-f - z_A) \cdot (y_B - y_A)}{(z_B - z_A)} + y_A \end{cases} \tag{7}$$

So, using the developed mathematical model, the point C position allows you to calibrate the setup so that this point coincides with the focus point F1 (in this case $y_C = 0$) for correct measurement, which is important in systems using ellipsoidal reflectors. When, according to the results of the experiment, it is established that with the given system parameters, the critical angle of the TIR θ_c value (the angle between the normal $\overline{n_1}(0;1)$ and the vector $\overline{R}$) has been reached, then its value can be determined by the formula:

$$\theta_c = a\cos\frac{\langle\overline{n_1},\overline{R}\rangle}{\|\overline{n_1}\|\cdot\|\overline{R}\|} \tag{8}$$

where

$$\langle\overline{n_1},\overline{R}\rangle = z_A - f,\ \ \|\overline{n_1}\| = 1,\ \ \|\overline{R}\| = \sqrt{(y_A)^2 + (z_A - f)^2} \tag{9}$$

The critical angle value of total internal reflection, determined using the mathematical apparatus (1)–(9), makes it possible to calculate the RI of a biological tissue sample under study:

$$RI_{BT} = RI_{ER}\cdot\sin\theta_c \tag{10}$$

3. Results and Discussion

The mathematical apparatus (1)–(10), as the basis of the specialized software developed by the authors, allows calculating the incidence angle ε_1/refractive index RI_{BT}/incidence point coordinates $A(y_A, z_A)$ depending on the input data set and the modeling purpose. We will demonstrate the simulation results showing the dependence of the incidence angle ε_1 of the laser beam on the ER side surface and the height h of its entry into the cavity of the ellipsoid on the predicted values of the BT RI, which, as indicated above, will be in the typical range of RI_{BT} values = 1.33…1.7. The RI_{BT} value step during modeling was 0.01, and to ensure the phenomenon of total internal reflection, the RI of transparent reflector material was RI_{ER} = 1.8. For modeling, it is also necessary to fix the focal parameter p, the increase or decrease of which characterizes ER scaling and depends on the BT sample scattering properties [34,39–41]. The CCD camera structural and optical parameters also determine it. Figure 5 characterizes the reflected beam tracing by the biological media at the total internal reflection and its impact on the ER opposite side surface with a focal parameter of 18 mm at different eccentricities.

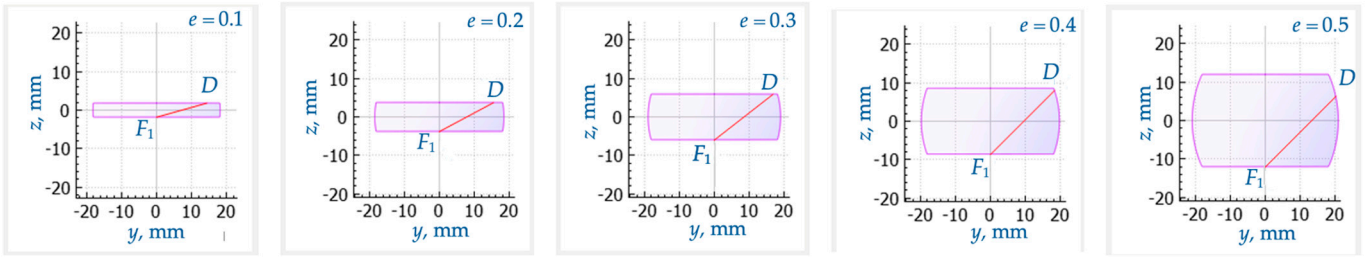


Figure 5. The rationale of transparent ellipsoidal reflector eccentricity range: (**a**) e = 0.1, (**b**) e = 0.2, (**c**) e = 0.3, (**d**) e = 0.4, (**e**) e = 0.5. Point D is the intersection point of the reflected beam with the opposite to the incident beam through the surface of the transparent reflector.

The eccentricity value range selection results show that the minimum (or maximum) value is 0.38 (or 0.57). It characterizes the impact of the reflected by the side surface beam on the edge of the second focal plane (or the absence of fulfillment of the total internal reflection phenomenon). Based on the design feature data for determining the BT RI with an ellipsoidal reflector method [34], the following simulation was carried out for the minimum e = 0.4 and the maximum e = 0.55 eccentricity values (Figure 6).

As seen in Figure 6, the ellipsoidal reflector's eccentricity significantly affects the measuring device's parameters. At the same time, the height of the beam entering the

ER (Figure 6b) is smaller. The higher RI of the BT under study agrees with the classical geometry of the law of refraction. At the same time, the dependence of the beam incident angle into the ER side part shows the presence of a specific fracture near the RI_{BT} = 1.5 at an eccentricity of 0.55 (as well as near the RI_{BT} = 1.65 at an eccentricity of 0.4), indicating the incident beam transition from the positive to the negative plane along the oz axis (Figure 4). The peak values of RI_{BT} correspond to the position of the incident beam at z = 0.

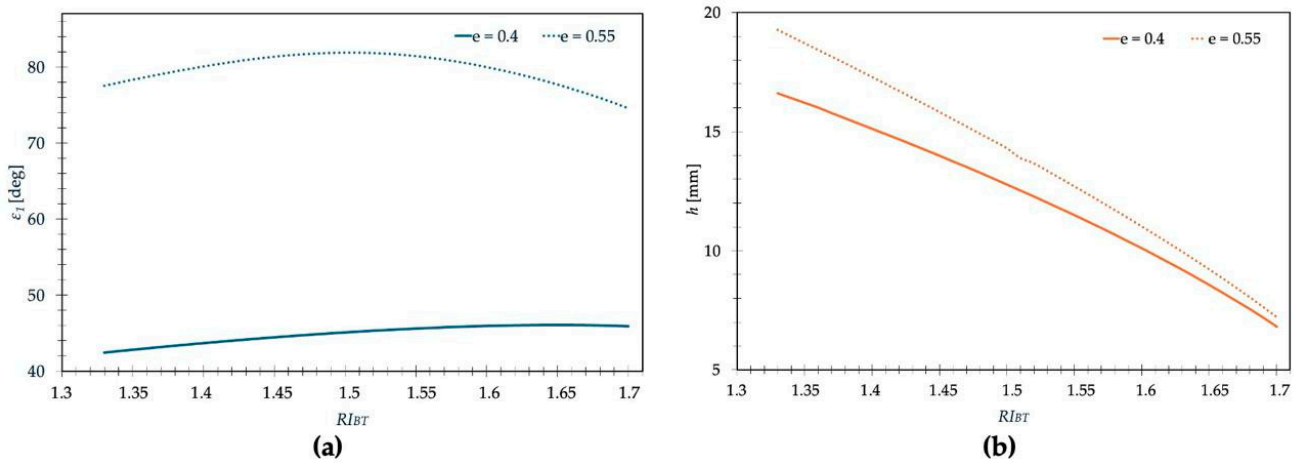


Figure 6. Dependence of the biological tissue RI RI_{BT} on the incidence angle ε_1 (**a**) and height h (**b**).

To ensure the correct determination of the incidence angles, which will be checked for the implementation of the TIR phenomenon, they will be practicalized using a stepper motor as a component of the electromechanical unit (EMU). To the electric current supplied by pulses, the stepper motor rotates to a certain specified angle, and the most common are two-phase (bipolar) motors with an angular displacement of 1.8°/step (200 steps per revolution) or 0.9°/step (400 steps per revolution). Since the ellipse generatrix is not a straight line, the incidence angle will begin to decrease after passing the equator of the ellipsoid (Figure 4a). Given these facts and the limitation of the eccentricity values' actual range, it will be more effective to use a motor with a smaller step angle to check the operation of the experimental model. For example, the Nema 17 model (Motion King, Changzhou City, China) has a step angle of 0.35°, which can ensure the determination of the RI of the test sample BT with accuracy up to 0.005. The dependence obtained in Figure 6b showed that even with larger RI_{BT} values, when the difference between the height of the beam entering the reflector decreases for the eccentricity extreme values, a micrometric control system of the height h vertical movement is sufficient.

Traditional methods for RI measuring, such as autocollimation, minimum deviation angle, and Abbe refractometer, are usually applied to transparent samples. The refractometry method obtains the deflection angle on the object's surface and cannot be used for multi-layer tissues. In contrast, the wavelength of the light source limits interferometric research methods, and researchers often face the problem of interferometer calibration accuracy. The wide application of optical coherence tomography is limited by the high cost of the equipment and the need to adjust the optical elements, and accuracy is lost in case of adjustment errors.

In this way, we characterized the effect of a typical range of the BT RI values on the position and incidence angle of the laser beam on the transparent ER side surface with a RI of 1.8. The literature analysis showed the lack of available technologies for the manufacture of glass ellipsoidal reflectors with mirror coating, which makes it impossible to conduct a practical study of the method's functioning and construct effective models for estimating the imaginary component of the complex RI of the BT. The authors consider a combined approach to solving the technological problems of obtaining a glass-transparent ER option.

This approach consists of filling a hollow ER made by trajectory copying [34] with an optically transparent material (Figure 7).

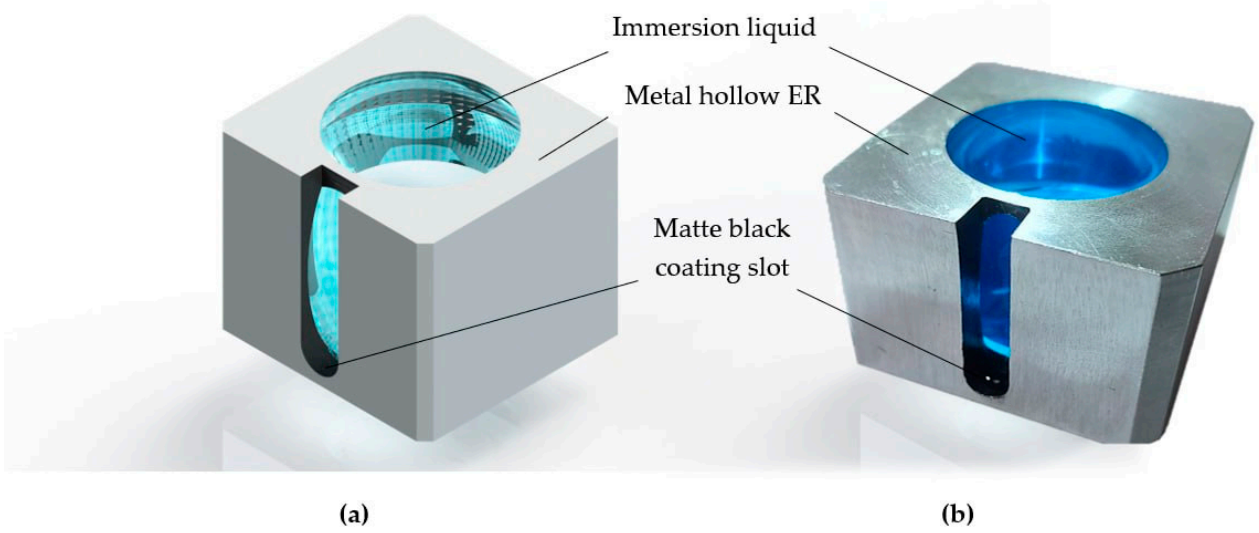


Figure 7. Liquid-filled ellipsoidal reflector: (**a**) 3D model, (**b**) product.

This design is characterized by a matte black coating slot performing the function of a ribbon-like element for introducing laser radiation into the cavity of a transparent ER. The key to making a liquid-filled ellipsoidal reflector is the correct selection of the liquid that will fill the hollow reflector with an internal mirror surface. Consider typical immersion liquid used in manufacturing, such as lenses. Sulfur in methylene iodide (CH_2I_2) solution has one of the highest refractive indices in liquids, 1.79 [42]. Liquids are less dense than solids, which explains why obtaining an RI greater than 2 is difficult. Anderson and Payne [42] state that selenium monobromide (Se_2Br_2) has a higher RI than pure liquid. The value of RI obtained by direct combination of elements is 1.96 ± 0.01, increasing to 2.02 when exposed to the atmosphere due to decomposition of the bromide with Se separation and reabsorption [43]. However, it is the organic immersion solution CH_2I_2 (diiodomethane) in comparison with other liquids with a high RI (for example, phenyldiodarsine $C_6H_5AsI_2$ with n = 1.85 and selenium monobromide) that is an excellent solvent for liquid compositions with salts, which contributes to obtaining an industrially available material with a greater index of refraction. The optical transparency of these liquids is relatively high in the visible and near-infrared spectra, and scattering is insignificant, which is especially important for isolating the imaginary component of the complex RI of light-scattering biological media. At the same time, the sulfur solution is very volatile, flammable, and poisonous; arsenic tribromide is not chemically neutral to glass and metals. It is poisonous by nature and reactive under the action of some minerals; methylene iodide is carcinogenic, selenium and its compounds are toxic, and selenium in the selenium monobromide solvent is unstable. Liquid iodine is not toxic, but its RI is 1.934 at 114 °C [44], which makes it impossible for an optical biomedical experiment. An alternative option is to use certified immersion oils, such as Cargille R.I. Liquid, Series M [Cargille-Sacher Laboratories Inc., Newark, NJ, USA], which are non-toxic organic compounds [43]. Gem Master R.I. liquid is also promising. Liquid [AGE Enterprise Co., Ltd., Bangkok, Thailand] with RI = 1.81 is used for testing the RI of gems in a gemological refractometer and is safe to use.

However, this option and producing a glass ellipsoid of revolution with mirror coating require developing a whole series of technological solutions, which form the direction of the authors' further research.

4. Conclusions

This paper introduces the theoretical fundamentals of a novel method for determining the RI of biological tissues using an ellipsoidal reflector. Based on total internal reflection phenomena, the method offers a unique approach to measuring the RI within the range of 1.33 to 1.7. The innovative design of the ellipsoidal reflector, coupled with a highly stable laser light source, ensures a high measurement accuracy.

The method's main advantage is the possibility of non-invasive measurement of the RI, which allows for in vivo research of biological tissues. The method also provides the possibility of registering scattered light, which allows for determining the imaginary part of the complex RI, which is essential for biomedical diagnostic applications.

The simulation results showed high accuracy in determining the critical angle of total internal reflection and the possibility of correct installation calibration for different RI values. The proposed approach to manufacture an ellipsoidal reflector filled with a liquid with a high RI opens new opportunities for further research and practical applications in biomedical optics.

The developed method and device design can significantly impact medical diagnostics. It could detect pathological changes in biological tissues early, improve patient outcomes, and reduce healthcare costs.

Author Contributions: Conceptualization, M.B.; validation, N.S.; formal analysis, P.K.; investigation, O.R.; resources, N.B.; data curation, O.R.; writing—original draft, N.B. and M.B.; writing—review and editing, P.K. and M.B.; visualization, N.S.; supervision, M.B. All authors have read and agreed to the published version of the manuscript.

Funding: Lublin University of Technology: FD-20/EE-2/312.

Institutional Review Board Statement: Not applicable.

Informed Consent Statement: Not applicable.

Data Availability Statement: The data presented in this study are available on request from the corresponding author.

Conflicts of Interest: The authors declare no conflict of interest.

References

1. Kirsch, A.; Hettlich, F. *The Mathematical Theory of Time-Harmonic Maxwell's Equations. Applied Mathematical Sciences*; Springer International Publishing: Cham, Switzerland, 2015; p. 337. [CrossRef]
2. Möller, K.D. Maxwell's Theory. In *Optics*, 2nd ed.; Springer: New York, NY, USA, 2007; pp. 205–247. [CrossRef]
3. Zhao, J.M.; Liu, L.H. Radiative Transfer Equation and Solutions. In *Handbook of Thermal Science and Engineering*; Kulacki, F., Ed.; Springer International Publishing: Cham, Switzerland, 2017; pp. 1–46. [CrossRef]
4. Liemert, A.; Reitzle, D.; Kienle, A. Analytical solutions of the radiative transport equation for turbid and fluorescent layered media. *Sci. Rep.* **2017**, *7*, 3819. [CrossRef]
5. Asllanaj, F.; Contassot-Vivier, S.; Liemert, A.; Kienle, A. Radiative transfer equation for predicting light propagation in biological media: Comparison of a modified finite volume method, the Monte Carlo technique, and an exact analytical solution. *J. Biomed. Opt.* **2014**, *19*, 015002. [CrossRef] [PubMed]
6. Das, N.; Chatterjee, S.; Kumar, S.; Pradhan, A.; Panigrahi, P.; Vitkin, I.A.; Ghosh, N. Tissue multifractality and Born approximation in analysis of light scattering: A novel approach for precancers detection. *Sci. Rep.* **2014**, *4*, 6129. [CrossRef]
7. Giannios, P.; Toutouzas, K.G.; Matiatou, M.; Stasinos, K.; Konstadoulakis, M.M.; Zografos, G.C.; Moutzouris, K. Visible to near-infrared refractive properties of freshly-excised human-liver tissues: Marking hepatic malignancies. *Sci. Rep.* **2016**, *6*, 27910. [CrossRef] [PubMed]
8. Sorensen, C.M.; Maughan, J.B.; Moosmüller, H. Spherical particle absorption over a broad range of imaginary refractive index. *J. Quant. Spectrosc. Radiat. Transf.* **2019**, *226*, 81–86. [CrossRef]
9. Sun, P.; Sun, H. Determination of the anisotropy complex refractive indices of chicken tissues in vitro at 650 nm. *J. Eur. Opt.Soc. Rapid Publ.* **2010**, *5*, 10030. [CrossRef]
10. Tomanic, T.; Rogelj, L.; Milanic, M. Robustness of diffuse reflectance spectra analysis by inverse adding doubling algorithm. *Biomed. Opt. Express* **2022**, *13*, 921–949. [CrossRef] [PubMed]
11. Gul, B.; Ashraf, S.; Khan, S.; Nisar, H.; Ahmad, I. Cell refractive index: Models, insights, applications and future perspectives. *Photodiagnosis Photodyn. Ther.* **2021**, *33*, 102096. [CrossRef]

12. Lin, L.; Li, H.; Xie, S. Linear method of determining the refractive index of biotissue. In Proceedings of the International Conference on Biomedical Optics, Wuhan, China, 25–27 October 1999. [CrossRef]
13. Jacques, S.L. Optical properties of biological tissues: A review. *Phys. Med. Biol.* **2013**, *58*, R37–R61. [CrossRef]
14. Poulon, F.; Mehidine, H.; Juchaux, M.; Varlet, P.; Devaux, B.; Pallud, J.; Abi Haidar, D. Optical properties, spectral, and lifetime measurements of central nervous system tumors in humans. *Sci. Rep.* **2017**, *7*, 13995. [CrossRef]
15. Zysk, A.M.; Adie, S.G.; Armstrong, J.J.; Leigh, M.S.; Paduch, A.; Sampson, D.D.; Nguyen, F.T.; Boppart, S.A. Needle-based refractive index measurement using low-coherence interferometry. *Opt. Lett.* **2007**, *32*, 385–387. [CrossRef]
16. Giannios, P.; Koutsoumpos, S.; Toutouzas, K.G.; Matiatou, M.; Zografos, G.C.; Moutzouris, K. Complex refractive index of normal and malignant human colorectal tissue in the visible and near-infrared. *J. Biophotonics* **2017**, *10*, 303–310. [CrossRef]
17. Wang, Z.; Tangella, K.; Balla, A.; Popescu, G. Tissue refractive index as marker of disease. *J. Biomed Opt.* **2011**, *16*, 116017. [CrossRef] [PubMed]
18. Khan, R.; Gul, B.; Khan, S.; Nisar, H.; Ahmad, I. Refractive index of biological tissues: Review, measurement techniques, and applications. *Photodiagnosis Photodyn. Ther.* **2021**, *33*, 102192. [CrossRef]
19. Sand, M.; Gambichler, T.; Moussa, G.; Bechara, F.G.; Sand, D.; Altmeyer, P.; Hoffmann, K. Evaluation of the epidermal refractive index measured by optical coherence tomography. *Ski. Res. Technol.* **2006**, *12*, 114–118. [CrossRef] [PubMed]
20. Zhou, Y.; Chan, K.K.; Lai, T.; Tang, S. Characterizing refractive index and thickness of biological tissues using combined multiphoton microscopy and optical coherence tomography. *Biomed. Opt. Express* **2013**, *4*, 38–50. [CrossRef] [PubMed]
21. Meng, Z.; Yao, X.S.; Yao, H.; Liang, Y.; Liu, T.; Li, Y.; Wang, G.; Lan, S. Measurement of the refractive index of human teeth by optical coherence tomography. *J. Biomed. Opt.* **2009**, *14*, 034010. [CrossRef] [PubMed]
22. Shirota, M.; van Limbeek, M.A.J.; Lohse, D.; Sun, C. Measuring thin films using quantitative frustrated total internal reflection (FTIR). *Eur. Phys. J. E* **2017**, *40*, 54. [CrossRef]
23. Kukharchuk, V.V.; Pavlov, S.V.; Holodiuk, V.S.; Kryvonosov, V.E.; Skorupski, K. Information Conversion in Measuring Channels with Optoelectronic Sensors. *Sensors* **2022**, *22*, 271. [CrossRef]
24. Shkilniak, L.; Zabolotna, N.; Pavlov, V.; Khomenko, Z.; Longyin, Y.; Gromaszek, K.; Kalizhanova, A.; Kozbakova, A. Photonic methods for normalizing the level of tissue microcirculation in the maxillo-facial region. In Proceedings of the Optical Fibers and Their Applications 2023, Lublin, Poland, 11–14 September 2023; Volume 12985. [CrossRef]
25. Lai, J.-C.; Zhang, Y.-Y.; Li, Z.-H.; Jiang, H.-J.; He, A.-Z. Complex refractive index measurement of biological tissues by attenuated total reflection ellipsometry. *Appl. Opt.* **2010**, *49*, 3235. [CrossRef]
26. Cheng, S.; Shen, H.Y.; Zhang, G.; Huang, C.H.; Huang, X.J. Measurement of the refractive index of biotissue at four laser wavelengths. In Proceedings of the Optics in Health Care and Biomedical Optics: Diagnostics and Treatment, Photonics Asia, Shanghai, China, 11–16 October 2020. [CrossRef]
27. Räty, J.; Peiponen, K.E. Inverse Abbe-method for observing small refractive index changes in liquids. *Talanta* **2015**, *137*, 143–147. [CrossRef] [PubMed]
28. Van Keuren, E.R. Refractive index measurement using total internal reflection. *Am. J. Phys.* **2005**, *73*, 611–614. [CrossRef]
29. Lai, J.; Li, Z.; Wang, C.; He, A. Effective refractive indices of biological tissues and its experimental determination. In Proceedings of the Optics in Health Care and Biomedical Optics: Diagnostics and Treatment II, 5630, Photonics Asia, Beijing, China, 11–16 October 2020. [CrossRef]
30. Morales-Luna, G.; Herrera-Domínguez, M.; Pisano, E.; Balderas-Elizalde, A.; Hernandez-Aranda, R.I.; Ornelas-Soto, N. Plasmonic biosensor based on an effective medium theory as a simple tool to predict and analyze refractive index changes. *Opt. Laser Technol.* **2020**, *131*, 106332. [CrossRef]
31. Li, H.; Xie, S. Measurement method of the refractive index of biotissue by total internal reflection. *Appl. Opt.* **1996**, *35*, 1793. [CrossRef] [PubMed]
32. Deng, Z.; Wang, J.; Ye, Q.; Sun, T.; Zhou, W.; Mei, J.; Zhang, C.; Tian, J. Determination of continuous complex refractive index dispersion of biotissue based on internal reflection. *J. Biomed. Opt.* **2016**, *21*, 15003. [CrossRef] [PubMed]
33. Malarenko, D.Y.; Bezugla, N.V.; Bezuglyi, M.O. Device for Measuring the Refractive Index of Biological Media. Patent UA124063C2, 14 July 2021.
34. Bezuglyi, M. Ellipsoidal Reflectors for Biological Media Light Scattering Photometry. In *Advanced System Development Technologies I. Studies in Systems, Decision and Control*; Bezuglyi, M., Bouraou, N., Mykytenko, V., Tymchyk, G., Zaporozhets, A., Eds.; Springer: Cham, Switzerland, 2023; Volume 511, pp. 119–154. [CrossRef]
35. Kurkjian, C.R.; Prindle, W.R. Perspectives on the History of Glass Composition. *J. Am. Ceram. Soc.* **1998**, *81*, 795–813. [CrossRef]
36. Wilk, S.R. *Sandbows and Black Lights: Reflections on Optics*; Oxford University Press: Oxford, UK, 2021.
37. Palik, E.D. (Ed.) *Handbook of Optical Constants of Solids, Part III*; Academic Press: Cambridge, MA, USA, 1998.
38. Bezuglyi, M.A.; Yarych, A.V.; Botvinovskii, D.V. On the possibility of applying a mirror ellipsoid of revolution to determining optical properties of biological tissues. *Opt. Spectrosc.* **2012**, *113*, 101–107. [CrossRef]
39. Bezuglyi, M.A.; Bezuglaya, N.V.; Helich, I.V. Ray tracing in ellipsoidal reflectors for optical biometry of media. *Appl. Opt.* **2017**, *56*, 8520–8526. [CrossRef] [PubMed]
40. Bezuglyi, M.; Bezuglaya, N.; Viruchenko, A. On the possibility of ellipsoidal photometry and Monte Carlo simulation to spatial analysis of biological media. In Proceedings of the IEEE 37th International Conference on Electronics and Nanotechnology (ELNANO), 18–20 April 2017. [CrossRef]

41. Bondariev, D.; Bezugla, N.; Komada, P.; Stelmakh, N.; Bezuglyi, M. Optical Properties of Light-Scattering Standards for CCD Photometry. *Sensors* **2023**, *23*, 7700. [CrossRef]
42. Anderson, B.W.; Payne, C.J. Liquids of High Refractive Index. *Nature* **1934**, *133*, 66–67. [CrossRef]
43. Laskar, J.M.; Kumar, P.S.; Herminghaus, S.; Daniels, K.E.; Schröter, M. High refractive index immersion liquid for superresolution 3D imaging using sapphire-based aplanatic numerical aperture increasing lens optics. *Appl. Opt.* **2016**, *55*, 3165–3169. [CrossRef]
44. Donaldson, A.; Caplin, A.D. The Optical Properties of Liquid Bromine and Iodine. *Philos. Mag. B* **1986**, *54*, 231–239. [CrossRef]

Disclaimer/Publisher's Note: The statements, opinions and data contained in all publications are solely those of the individual author(s) and contributor(s) and not of MDPI and/or the editor(s). MDPI and/or the editor(s) disclaim responsibility for any injury to people or property resulting from any ideas, methods, instructions or products referred to in the content.